Journal of Harbin Engineering University
ISSN: 1006-7043
Vol 44 No. 10
October 2023

Fabrication and Testing of Small Scale Helical Wind Turbine

Kumaresan Cunden[1] , Professor Freddie Inambao[2*]
[1,2*]:Department of Mechanical Engineering, University of KwaZulu-Natal
Howard College, Durban, 4000, South Africa
[2*]https://orcid.org/0000-0001-9922-5434
[2*]https://www.scopus.com/authid/detail.uri?authorId=55596483700

Abstract
Wind energy is one of the most abundant resources being exploited with wind turbines having the traditional horizontal axis wind turbine configuration. Traditional horizontal axis configurations are being utilized in onshore and offshore wind farms; however, the investigation of vertical axis wind turbine configurations has been increasing. The following study aims to investigate the design of a helical vertical axis wind turbine. A small-scale helical vertical axis wind turbine was designed based on previous investigations and research. The turbine was tested at wind speeds ranging from 7.5 m/s to 9.5 m/s. The results showed that the wind turbine was in good agreement with numerical simulations under typical environmental conditions.
Keywords: *Vertical Axis Wind Turbine, Helical Wind Turbine, Small Scale Wind Turbine Blade Design*

NOMENCLATURE AND ABBREVIATIONS

AR	Aspect Ratio	P_m	Mechanical Power
A_S	Surface Area of Turbine	RPM	Revolutions per Minute
A_T	Wind Tunnel Test Section Area	T	Torque
A_ω	Swept Area	VAWT	Vertical Axis Wind Turbine
B	No. of Turbine Blades	U_c	Corrected Wind Speed
B_f	Blockage Factor	U_f	Wind Speed without Turbine
B_R	Blockage Ratio	U_t	Wind Speed with Turbine
c	Blade chord length	U_∞	Freestream Wind Speed
C_P	Coefficient of Power	σ	Solidity Ratio
D	Turbine Diameter	δ	Helix Angle
DC	Direct Current	ρ	Density of Fluid
H	Turbine Height	ω	Rotational Speed
P_f	Power of the fluid	ώ	Turbine Blade Wrap

Introduction

Wind energy is one of the most abundant resources being exploited with wind turbines having the traditional horizontal axis wind turbine configuration. The onshore turbines have been in commercial operation globally in many electrical grids for many years, [1], [2]. Recently wind turbines have been migrating to offshore locations to harness greater resource availability and potential due to a lack of environmental obstructions, [3]–[5].

Traditional horizontal axis configurations are being utilized in onshore and offshore wind farms; however, the investigation of vertical axis wind turbine configurations has been increasing. One of the main advantages of vertical axis turbines, in comparison to horizontal axis turbines, is that they are not as limited to the direction of wind flow and can operate under crosswind conditions.

The following study aims to investigate the design of a helical vertical axis wind turbine that was described in [6]. The study was conducted to determine the characteristics of the turbine when subjected to wind loading forces within a controlled environment. The empirical investigation aimed to identify the start up wind speed as well as how the simulation results compared to a small scale model test of the

design. The stud provides an overview of the fabrication process and the materials used for the construction of the small scale turbine which included support struts.

The following study aims to investigate the design of a helical vertical axis wind turbine. The layout of this article consists of the methodology, the turbine design parameters, the fabrication process of the small-scale turbine, a numerical simulation of the turbine, the experimental configuration followed by the results, discussions, and conclusions of the findings of the investigation.

1 Methodology

The following small-scale helical axis wind turbine was designed based on investigations and finds from the research conducted by Cunden and Inambao in [1] and [2]. The design has focused on a Selig 1406 17% thickness blade profile which is an asymmetrical blade profile. The results from [6] investigations showed that the profile had performed favourably in comparison to the NACA symmetrical profiles which were assessed. The fabrication of the turbine is detailed in Section 0.

The turbine was constructed and tested in the wind tunnel which was designed and constructed in [8]. The power was measured using a DC motor which was logged with a ChipKit uC32 microcontroller configured to log the current, voltage, and electrical power of the turbine at the rotor. A tachometer was developed with the aid of a digital hall effect sensor to measure the turbine rotational speed. The description of the experimental setup is detailed in[8]. This experimental setup was used to assess the rotational speed of the direct drive wind turbine and relate the rotational speed to that of the power output of the scaled modelled turbine which provided insight into the larger scale wind turbine.

2 Turbine Design

Horizontal axis wind turbines (HAWT) represent the most common wind turbine design which is found globally. These turbines traditionally consist of three blades with complex blade geometry and design, however, they also have a relatively high generation performance, [9]. One of the disadvantages of these turbines is that they have limited the direction of wind incoming from the turbine. A vertical axis wind turbine (VAWT), in comparison to the HAWT, has a simpler blade geometry and has the advantage of being a cross-flow turbine and is not limited to the lateral direction of incoming wind flow.

Figure 1 represents a basic discretization of a helical axis wind turbine which was used as the basis for the fabrication of the small-scale wind turbine evaluated for this study.

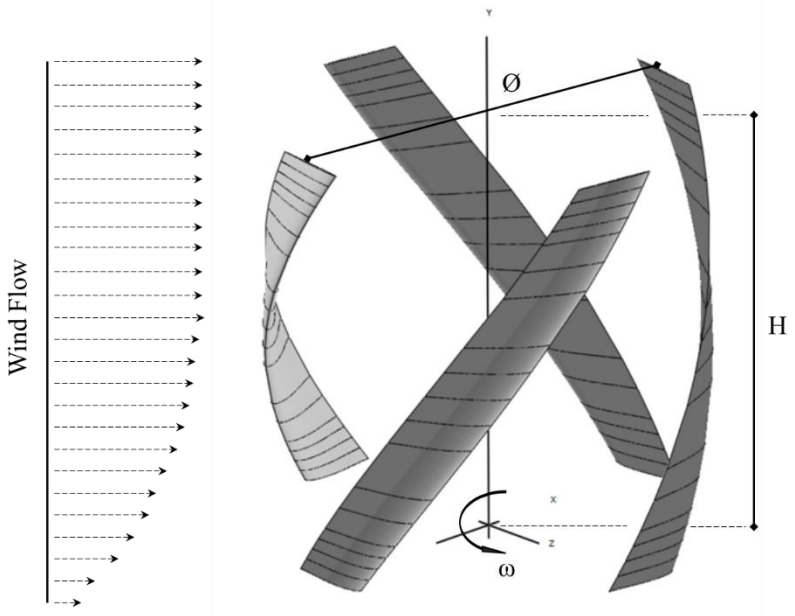

Figure 1: Helical Vertical Axis Wind Turbine

The turbine was designed based on the constraints of the wind tunnel which was designed and constructed by Cunden, K, [8] to test the small-scale helical wind turbine. Further investigation results indicate that the aspect ratio (AR) relationship to solidity directly affects the turbine power output. The following study utilizes an AR or 1 to maximize the swept area (A_ω) of the turbine.

The turbine was limited based on the wind tunnel testing chamber height. Equation (1) shows the relationship of the turbine height in comparison to the turbine radius known as the turbine's aspect ratio. The resultant turbine radius is 87.5 mm and the diameter (D) is 175 mm using a turbine height of 175 mm.

$$AR = \frac{H}{2R} \quad (1)$$

Using a solidity ratio (σ) of 25% from the results of the study which was conducted in [6] the blade chord length (c) was calculated based on Equation (2) resulting in a blade chord length of 34.5 mm.

$$\sigma = \frac{Bc}{\pi D} \quad (2)$$

The blade wrap of a VAWT describes the number of the turbine's blades that are in contact with the fluid. The results from [7] indicated that four turbine blades with a 100% blade wrap had resulted in a smoother torque profile on the rotor shaft. Using the above constraints and results the helix angle (δ) was calculated to be 51.85°.

$$\acute{\omega} = \frac{BH}{\pi D \tan\delta} \quad (3)$$

The tip speed ratio (λ) is the relationship of the turbine rotational speed (ω) in comparison to the fluid velocity (V) shown in Equation (4). This parameter is used to evaluate the turbine's parameters in the numerical solver from the results obtained from the testing of the small-scale turbine within the wind tunnel.

$$\lambda = \frac{R\omega}{V} \quad (4)$$

The power in the fluid (P_f) is described in Equation (5) where the power is a function of the density (ρ) of the fluid, the wetted area (A_ω), the freestream fluid velocity (U_∞).

$$P_f = \frac{1}{2}\rho A_\omega {U_\infty}^3 \quad (5)$$

The mechanical power (P_m) is described in Equation (6) which can be related to Equation (5). Using the relation of the two equations and understanding the rotational speed of the turbine by using Equation (4) the torque can be calculated.

$$P_m = T\omega \quad (6)$$

The coefficient of power (C_P) for a wind turbine is the ratio of the mechanical power which is extracted by the turbine is about the amount of power within the fluid shown in Equation (7). The turbine maximum C_P is constrained by the Betz limit which is the theoretical maximum limit a turbine may extract from the fluid, [7].

$$C_P = \frac{P_m}{P_f} \quad (7)$$

Usually, turbine rotors are tested within wind tunnels and are near the test section walls which is not the case when operating in natural environments. This challenge arises from a blockage effect that has two main components the solid blockage and the wake blockage. The solid blockage is a result of the turbine's projected blade area impeding the wind tunnel flow and the wake blockage is the wake effect of the turbine which may not dissipate the wake energy as would be in natural conditions, [10].

When testing the VAWT within a wind tunnel the blockage ratio (B_R) was needed to correct the freestream fluid velocity (U_∞) due to the effect of the projected surface area of the wind turbine (A_S) impeding the wind flow through the wind tunnel test section (A_T). The relationship is represented in Equation (8), [11].

$$B_R = \frac{A_S}{A_T} \quad (8)$$

Research conducted by [11] notes where the blockage ratio exceeds 10% the results which are found are required to be corrected by the blockage factor. Various methods have been developed to calculate the blockage effect for wind tunnel testing. The research conducted by [12] derived correction factors related to drag and pressure coefficients to develop a semi-empirical factor whereas [13] suggested a simple method using 25% of B_R to correct the freestream velocity. Methods that were proposed by [14] had successfully built on the finds of [12] to a Savonius

drag-type turbine. Investigations from [15] proposed correction methods based on utilizing the actuator disk theory and correcting thetip speed ratio (λ) and coefficient of power (C_P) as shown in Equation (4) and Equation (7) respectively by using the blockage factor (B_f) shown in Equation (9).

$$B_f = \frac{U_t}{U_f} \tag{9}$$

The blockage factor proposed by [15] relates the wind tunnel flow velocity with the turbine rotor (U_t) to the wind tunnel flow velocity without the turbine rotor (U_f)

Methods proposed by [13] were also adopted to correct the wind velocity incoming the turbine rotor with Equation 10. The factor (ε_t) is described as 25 % of the blockage ratio described in Equation (8). These factors were used in the correction of the test results data detailed in Section 5 of the study.

$$U_c = U_\infty(1 + \varepsilon_t) \tag{9}$$

based on the consolidation of the above design parameters.

Table 1 shows the final turbine rotor specifications used for the fabrication of the helical turbine

Table 1: Turbine Specifications

Design Parameters	Detail
Aspect Ratio (AR)	1
Turbine Diameter (D)	175 mm
Turbine Height (H)	175 mm
Solidity (σ)	25 %
No. of Blades (B)	4
Blade Chord Length (c)	34.5 mm
Blade Wrap (ώ)	100 %
Helix Angle (δ)	51.85°

The specifications from Table 1 and the correction factors were used in the fabrication of the turbine and the analysis of the results from the wind tunnel testing.

3 Fabrication Process

The following section of the study details the fabrication process of the helical VAWT highlighting the blade discretization and strut design for the turbine. One of the challenges experienced when fabricating the turbine was blade manufacturing. Due to the twist angle of the helical profile, the turbine blade was segmented.

A three-dimensional (3D) printer was used to fabricate the turbine blades, couplings, bearing mountings, and upper and bottom struts. The fabrication process of a turbine blade is described in [16]–[18] of traditional HAWT blades. The turbine blades are hollow and consist of an outer shell that forms the aerodynamic shape to produce a resultant lift force. The helical blade which was designed to have a total helix angle of 51.85° was sectioned into five pieces of the same height and interlocked resulting in a piecewise helix angle of 10.37°

Figure 2 (a) depicts one of the five designed blade segments and Figure 2 (b) depicts a partial and fully fabricated blade segment. The partially fabricated blade segment was captured to illustrate the hollow nature of the turbine blade.

Figure 2 (a): Blade Segment

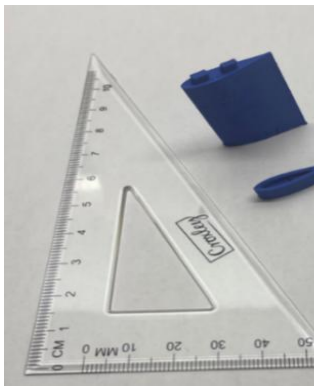

Figure 2 (b): Blade Segment

The blades were sectioned into 5 interlocking pieces which were stacked on top of one another to form a full turbine blade as shown in Figure 3 (a). The interlocking of the blade segments was fabricated to have a tolerance of ±0.1 mm to ensure a tight fit when assembled which is shown in Figure 3 (b).

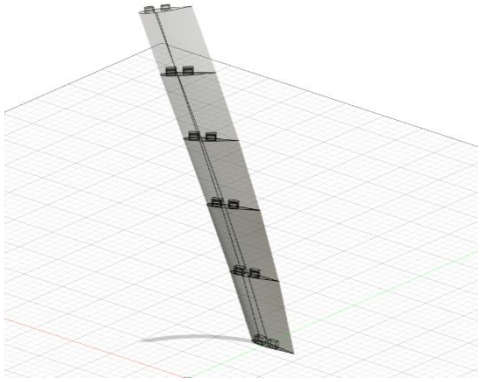

Figure 3 (a): Turbine Blade Assembly

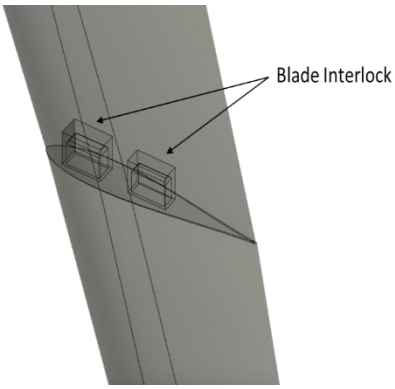

Figure 3 (b): Blade Interlock

The blades were assembled and fixed to an upper and lower strut with a center tube shaft which was used to stabilize the turbine and transfer the extracted energy to be useful mechanical energy for power generation. Figure 4 depicts the fully assembled turbine prototype for testing.

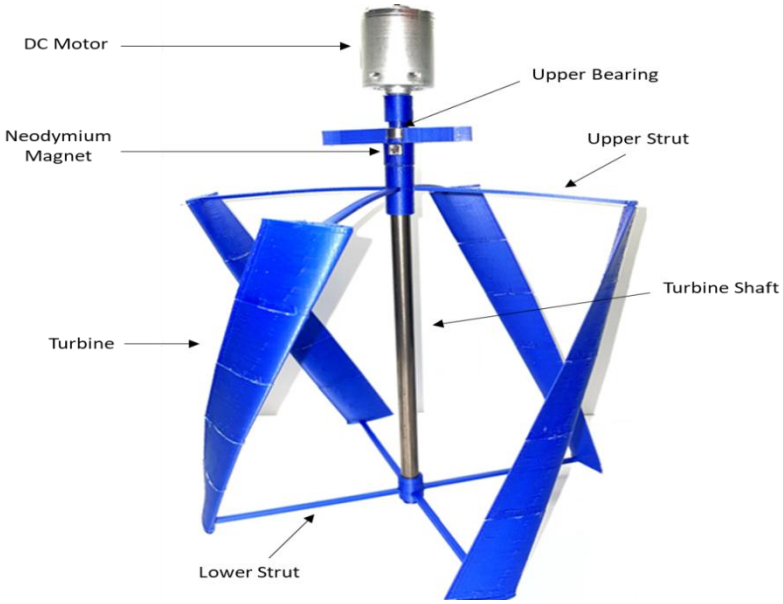

Figure 4: Turbine Assembly

The turbine and coupling components were assembled and tested within a wind tunnel at wind speeds of 7.5 m/s to 9.5 m/s.

4 Experimental Configuration

The following section of the study elaborates on the configuration of the experimental setup as well as the instrumentation used for the investigation of the VAWT in the wind tunnel setup. Figure 5 illustrates the experimental set-up of the VAWT within the wind tunnel as well as the DC motor coupling used to measure the power output from the turbine.

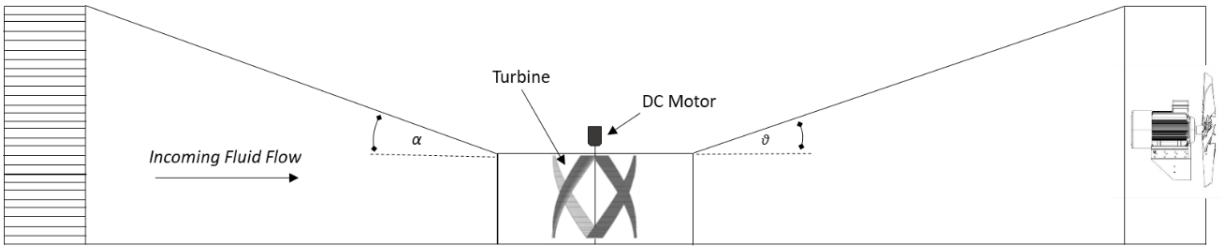

Figure 5: Experimental Set-up

Figure 6 shows the instrumentation and other devices used to log the experimental data from the designed VAWT. The turbine was connected to the DC motor using a hexagonal socket and a tight-fit connection to the DC motor shaft. This was where some losses occurred as a result of inertia and torque of the DC motor as well as frictional losses through the coupling system to the motor shaft. The voltage sensor was sued to determine the output voltage and current to calculate the power output of the turbine. The Hall effect sensor was used to measure the rotational speed of the turbine shaft by counting the pulses generated by the Neodymium magnet. The readings were processed and logged by the ChipKit uC32 microcontroller and saved to the PC for post-processing.

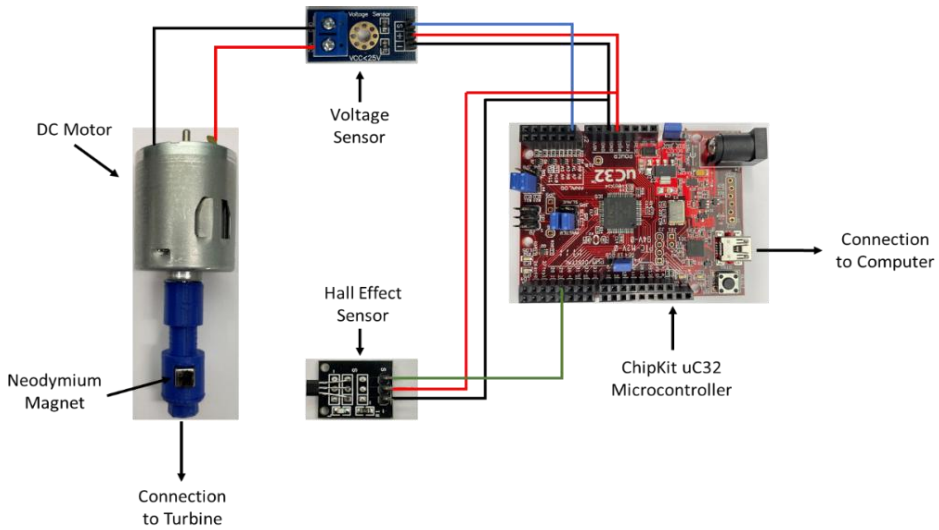

Figure 6: Instrumentation

The above instrumentation was interfaced with a computer via a serial communication cable. The results were logged in 5-second intervals to average out instantaneous fluctuations at the rotor shaft which may have not been accurately captured due to feedback and resolution from sensors.

5 Results And Discussion

The following section of the study elaborates on the results of the wind tunnel testing for the designed VAWT. Three tests were conducted by varying the wind tunnel wind speed by 0.5 m/s and the results were logged in 5-second intervals and allowed to settle for 5 minutes.

Figure 7 below shows the power measurements, of the three averaged tests which were conducted, in comparison to the rotational speed (RPM) at the rotor of the turbine.

A numerical simulation was performed for the turbine utilizing a double multiple stream tube analysis. The numerical simulation had the specifications which are shown in Table 2 below.

Table 2: Simulation Parameters

Simulation Parameters	Detail
Temperature	20 °C
Density of Air	1.204 kg/m^3
Mach Number	0.028
Dynamic Viscosity	1.825 x 10^{-5} kg/ms
Wind Speed	7.5 / 8 / 8.5 / 9 / 9.5 m/s

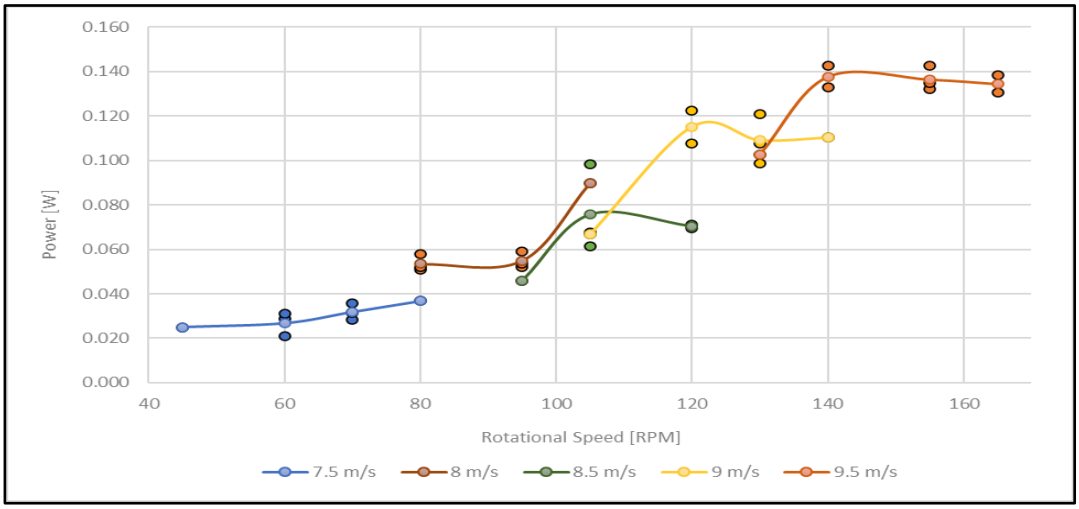

Figure 7: Experimental Results

Figure 8 represents the corrected values of the power measurements considering Equations (9) and (10) factoring in the blockage effects of the turbine in the wind tunnel. The freestream wind speed and the corrected power were used to calculate and plotted against the measured data.

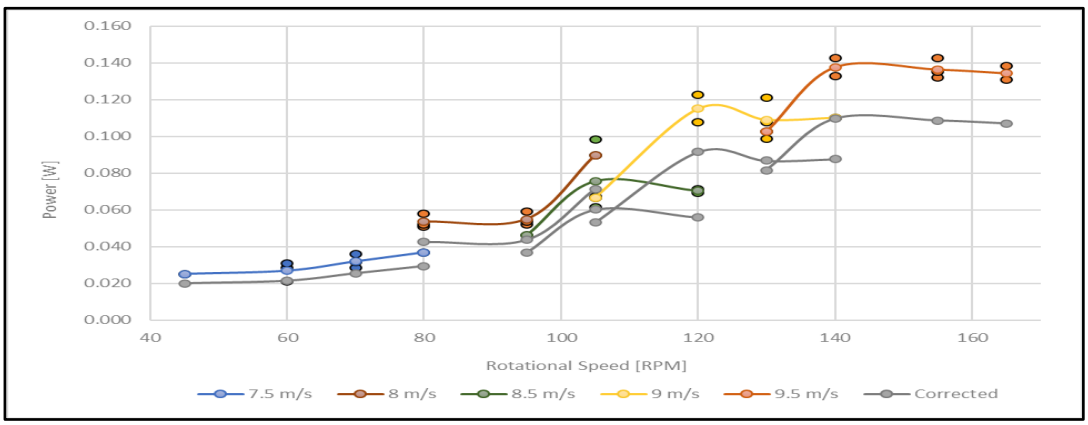

Figure 8: Experimental Results Corrected

Figure 9 shows the results of the wind tunnel test in comparison to a numerical simulation performed for the turbine. The measured results are in good relation to that of the freestream numerical solver results after utilizing the correction methods. The variations shown may be a result of vibration due to misalignment of turbine bearings and vibrations of the motor used whilst in operation.

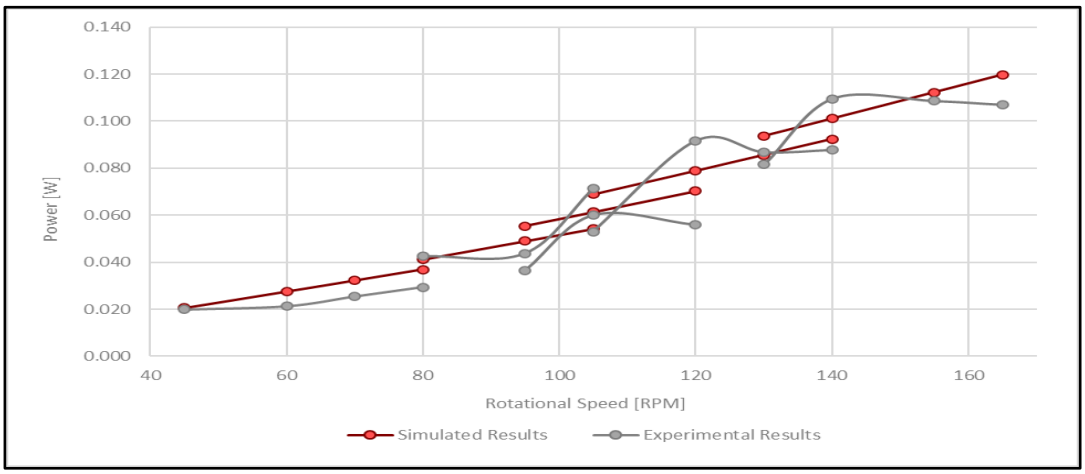

Figure 9: Measured compared to Simulation

The above results illustrate the turbine design may be developed for practical operations onshore and offshore for wind speeds having a mean of 9 m/s. Challenges may arise from turbine blade manufacturing as the helical VAWT requires a twist angle which may be challenging for casting a single blade. One of the solutions may be to fabricate the blade in segments. Further investigations should be conducted into the fabrication of large-scale VAWTs.

6 Conclusions

A small-scale turbine rotor was designed using the formula described and was tested in a wind tunnel over a varying speed of 7.5 m/s to 9.5 m/s. The turbine blades were fabricated in sections due to the helical nature of the blade. The turbine output power and rotational speed were measured at each wind speed. A numerical simulation was performed considering an unbounded condition of flow which were in good comparison to the measured results after utilizing the appropriate correction factors. The torque profile of the turbine may be calculated, at different wind speeds, by utilizing the measured power and turbine rotational speed. Further research should be considered on varying strut designs and positions as well larger turbines with smaller segments for the turbine blades.

References

[1] K. Umoh and M. Lemon, “Drivers for and barriers to the take up of floating offshore wind technology: A comparison of Scotland and South Africa,” Energies (Basel), vol. 13, no. 21, 2020, doi: 10.3390/en13215618.

[2] British Petroleum (BP), “Statistical Review of World Energy 2021,” 2021.

[3] M. Hannon, E. Topham, J. Dixon, D. McMillan, and M. Collu, “Offshore Wind, Ready to Float? Global and UK Trends in the Floating Offshore Wind Market,” 2019. doi: 10.17868/69501.

[4] H. Díaz and C. Guedes Soares, “Review of the current status, technology and future trends of offshore wind farms,” Ocean Engineering, vol. 209, p. 107381, 2020, doi: https://doi.org/10.1016/j.oceaneng.2020.107381.

[5] S. Loughney, J. Wang, M. Bashir, M. Armin, and Y. Yang, “Development and application of a multiple-attribute decision-analysis methodology for site selection of floating offshore wind farms on the UK Continental Shelf,” Sustainable Energy Technologies and

Assessments, vol. 47, p. 101440, 2021, doi: https://doi.org/10.1016/j.seta.2021.101440.

[6] F. L. Inambao and K. Cunden, “Offshore Vertical Axis Wind Turbine Simulation,” International Journal of Mechanical and Production Engineering Research and Development, vol. 11, no. 2, pp. 187–204, 2021.

[7] K. Cunden, “Design of a Novel Hydrokinetic Turbine for Ocean Current Power Generation,” University of Kwa-Zulu of Natal, 2015.

[8] K. Cunden and F. L. ; Inambao, “Design, Construction and Testing of a Low-Speed Wind Tunnel,” International Journal of Mechanical and Production Engineering Research and Development, vol. 11, no. 6, pp. 237–256, 2021.

[9] D. Han, Y. G. Heo, N. J. Choi, S. H. Nam, K. H. Choi, and K. C. Kim, “Design, fabrication, and performance test of a 100-W helical-blade vertical-axis wind turbine at low tip-speed ratio,” Energies (Basel), vol. 11, no. 6, pp. 1–17, 2018, doi: 10.3390/en11061517.

[10] J. B. ; Barlow, W. H. ; Rae, and A. Pope, Low-Speed Wind Tunnel Testing, Third. Toronto: John Wiley & Sons, 1999.

[11] E. Bešlagić, S. Lemeš, and F. Hadžikadunić, “Procedure for Determining the Wind Tunnel Blockage Correction Factor,” in New Technologies, Development and Application III, I. Karabegović, Ed., Cham: Springer International Publishing, 2020, pp. 331–339. doi: 10.1007/978-3-030-46817-0_38.

[12] E. C. ; Maskell, “A Theory of the Blockage Effects on Bluff Bodies and Stalled Wings in a Closed Wind Tunnel,” London, 1963.

[13] A. Pope and J. . J. ; Harper, Low-Speed Wind Tunnel Testing. New York: John Wiley & Sons, 1966.

[14] A. J. Alexander and B. P. Holownia, “Wind tunnel tests on a savonius rotor,” Journal of Wind Engineering and Industrial Aerodynamics, vol. 3, no. 4, pp. 343–351, 1978, doi: 10.1016/0167-6105(78)90037-5.

[15] A. S. ; Bahaj, A. F. ; Molland, J. R. ; Chaplin, and W. M. J. ; Batten, “Power and thrust measurements of marine current turbines under various hydrodynamic flow conditions in a cavitation tunnel and a towing tank,” Renew Energy, vol. 32, no. 3, pp. 407–426, 2007, doi: 10.1016/j.renene.2006.01.012.

[16] C.-H. Ong and S. Tsai, “Design, Manufacture andTesting of A Bend-Twist D-spar,” Stanford CA, 1999.

[17] P. S. ; Veers et al., “Trends in the Design, Manufacture and Evaluation of Wind Turbine Blades,” Wind Energy, vol. 6, pp. 245–259, 2003, doi: 10.1002/we.90.

[18] D. Murray, Robynne E.; Snowberg, D. Berry, R. Beach, S. Rooney, and D. Swan, “Manufacturing a 9-Meter Thermoplastic Composite Wind Turbine Blade,” in American Society for Composites, West Lafayette, Indiana: National Renewable Energy Laboratory (NREL), 2017.